# Degenerate and nondegenerate parametric excitation in yttrium iron garnet nanostructures

H. Merbouche,[1,*] P. Che,[2] T. Srivastava,[3] N. Beaulieu,[4] J. Ben Youssef,[4] M. Muñoz,[5]
M. d'Aquino,[6] C. Serpico,[6] G. de Loubens,[3] P. Bortolotti,[2] A. Anane,[2] S.O. Demokritov,[1] and
V.E. Demidov[1]

[1]*Institute for Applied Physics, University of Muenster, Münster, Germany*
[2]*Laboratoire Albert Fert, CNRS, Thales, Université Paris-Saclay, Palaiseau, France*
[3]*SPEC, CEA, CNRS, Université Paris-Saclay, Gif-sur-Yvette, France*
[4]*LabSTICC, UMR 6285 CNRS, Université de Bretagne Occidentale, Brest, France*
[5]*Instituto de Tecnologías Físicas y de la Información (CSIC), Madrid, Spain*
[6]*Department of Electrical Engineering and ICT, University of Naples Federico II, Naples, Italy*

We study experimentally the processes of parametric excitation in microscopic magnetically saturated disks of nanometer-thick yttrium iron garnet. We show that, depending on the relative orientation of the parametric pumping field and the static magnetization, excitation of either degenerate or nondegenerate magnon pairs is possible. In the latter case, which is particularly important for applications associated with the realization of computation in the reciprocal space, a single-frequency pumping can generate pairs of magnons whose frequencies correspond to different eigenmodes of the disk. We show that, depending on the size of the disk and the modes involved, the frequency difference in a pair can vary in the range 0.1–0.8 GHz. We demonstrate that in this system, one can easily realize a practically important situation where several magnon pairs share the same mode. We also observe the simultaneous generation of up to six different modes using a fixed-frequency monochromatic pumping. Our experimental findings are supported by numerical calculations that allow us to unambiguously identify the excited modes. Our results open new possibilities for the implementation of reciprocal-space computing.

## I. INTRODUCTION

The field of magnonics aims to use spin waves (SWs) as information carriers to perform radio-frequency (rf) processing as well as classical and neuromorphic computing [1–4]. Indeed, spin waves (and their quanta—magnons) are a promising alternative to charge carriers because of their low energy, short wavelength, and easily attainable nonlinear dynamics. These characteristics make them particularly suited for the implementation of new computing schemes that take advantage of the massive parallelization of operations in the frequency space and of the intrinsic hyperconnectivity in the reciprocal space (**k** space) due to nonlinear spin-wave interactions [5–11]. Dynamic magnetic systems can thus be seen as a neural network whose nodes are SW modes that are interconnected by nonlinear magnon-magnon interactions in the **k** space. The inputs

and outputs of such a network can be accessed and read either in the frequency space [10,11], or by the use of a real-space separation, through propagation and wave interference [5,6,8]. Implementation of such schemes requires the excitation and manipulation of many modes in small magnetic structures. This can be achieved by the use of parametric processes [12], where a photon or a magnon at frequency $2f$ splits into two magnons at frequencies $f - \delta f$ and $f + \delta f$. The splitting can be degenerate ($\delta f = 0$) or nondegenerate ($\delta f \neq 0$). The degenerate process has been the most studied to excite SW modes in a broad range of materials and systems, including extended films [12–18] and microwaveguides and nanowaveguides [19–22] as well as magnetic nanocontacts [23], magnetic tunnel junctions [24], microdots and nanodots of permalloy [25–27], and yttrium iron garnet (YIG) [28]. In contrast to direct linear excitation [29], it allows the efficient excitation of modes with the use of a uniform dynamic magnetic field irrespective of the mode spatial profile [25,28]. On the other hand, excitation of nondegenerate pairs has been observed only in extended micrometer-thick YIG films

_____
*Corresponding author: hugo.merbouche@cea.fr

[30] and in confined metallic structures in a vortex state [31,32]. In the latter case, the nondegeneracy was shown to open the possibility to cross-stimulate mode excitation with the use of multiple parametric pumps, thus effectively implementing an interconnected recurrent neural network capable of classifying microwave signals [11].

So far, nondegenerate parametric excitation has relied on the specific configuration with a strong dipolar dip in the dispersion relation, which was achieved in either micrometer-thick YIG films [30] or in ferromagnetic structures in the vortex ground state at zero magnetic field [31] or low static magnetic field [32]. In these configurations, the dispersion relation is such that the frequencies of the low-order magnon modes are about twice the frequencies of higher-order modes. The low-order modes can be efficiently excited with the use of the direct inductive mechanism and then magnon pairs are generated through the parametric process [30,33]. Such favorable configurations are not possible in nanometer-thick films of magnetic insulators with low magnetization, such as YIG. However, YIG is a key material in magnonics due to its extremely low magnetic damping $\alpha$ [34–36], nearly 2 orders of magnitude smaller than that in metallic ferromagnets. Since low damping strongly lowers the threshold of nonlinear processes [12,33], finding a method to excite nondegenerate magnon pairs in ultrathin-film YIG structures is an important step in the development of magnonic computing schemes based on nonlinear interactions.

In this study, we demonstrate experimentally that both degenerate and nondegenerate parametric processes can be realized in the same magnetically saturated microscopic ultrathin YIG disk by simply varying the direction of the parametric pumping field with respect to the static magnetization. When the field is applied parallel to the static magnetization (parallel pumping), a photon of the pumping field splits into a degenerate magnon pair at half the frequency, as expected. However, when the field is applied transverse to the static magnetization (transverse pumping), it nonresonantly excites a magnon, which then splits into a magnon pair that is typically nondegenerate. We show that the efficiency of this process is comparable to the efficiency of the parallel-pumping process, which makes it attractive for technical application. Additionally, the nondegenerate parametric excitation via the generation of nonresonant magnons is not limited by the frequencies of the resonant modes of the system. As a result, this technique is much more flexible than resonant three-magnon scattering schemes and does the not require the strong dipolar dip that strongly limited its practical use in key materials such as thin YIG. These findings greatly facilitate the implementation of nondegenerate parametric processes for the excitation and control of magnetic modes. They also bolster the realization of promising **k**-space computing schemes using attractive magnonic materials such as thin YIG.

## II. EXPERIMENT

Figure 1(a) shows the schematics of the experiment. A 52-nm-thick YIG film grown by liquid-phase epitaxy on a Gadolinium Galium Garnet (GGG) substrate is patterned by electron-beam lithography to define disks with a diameter $D$ ranging from 500 nm to 2 µm. A 150-nm-thick and 4-µm-wide Au antenna is fabricated on top of the YIG structures to apply a uniform dynamic magnetic field $h_{rf}$ induced by the rf current $i_{rf}$ in the antenna. The static magnetic field $H_0$ is applied in the plane such that it is either transverse ($\varphi = 90°$) or parallel ($\varphi = 0$) to the dynamic field $h_{rf}$. The excitation is applied in the form of 500-ns-long pulses with a repetition period of 1 µs to monitor the transient dynamics of the different parametric processes. The magnetization dynamics is detected by microfocus Brillouin-light-scattering (BLS) spectroscopy [37], which yields a signal (BLS intensity) proportional to the intensity of the magnetization dynamics at the position of the probing laser spot [see Fig. 1(a)]. Note that the dynamic magnetization profile of nonuniform modes can exhibit a
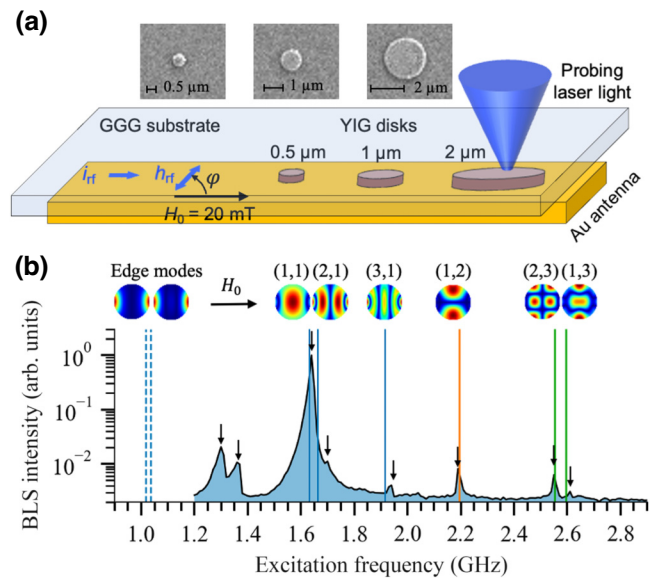


FIG. 1.   (a) Experimental setup. YIG disks with a thickness 52 nm and a diameter of 0.5, 1, and 2 µm are excited by a dynamic field $h_{rf}$ created with the use of a 4-µm-wide antenna. The static magnetic field $H_0$ is applied either parallel or transverse to the dynamic field. Insets show electron-microscope images of the disks taken before the antenna was fabricated. (b) Characterization of the eigenmode spectrum of a 0.5-µm disk. The graph shows the intensity of the dynamic magnetization as a function of the excitation frequency under conditions of direct linear excitation ($\varphi = 90°$) with $P = 0.2$ mW at $H_0 = 20$ mT. Arrows mark the frequencies of the detected resonant peaks. Vertical lines mark the calculated frequencies of the eigenmodes. The calculated spatial profiles of the modes are shown close to the corresponding lines. These profiles present the absolute value of the out-of-plane component of the dynamic magnetization.

change of the sign over the area of the probing spot. This leads to reduced sensitivity of the BLS apparatus to modes with certain spatial symmetries due to the spatial averaging over the opposite phases of the magnetization dynamic profiles. Therefore, the measurements are performed with the spot shifted from the center of the disk by half its radius [see Fig. 1(a)], which allows simultaneous observation of symmetric and antisymmetric modes of the disk. The probing light is focused onto the YIG disks through the sample substrate by means of a corrected objective lens with a magnification of 100 and a numerical aperture of 0.85. The BLS measurements are performed with simultaneous spectral and temporal resolution. The latter is realized by synchronizing the detection of the scattered light with the excitation pulses.

We first characterize the spectrum of resonant SW modes by using a direct low-amplitude linear excitation. We apply the static field transverse to the dynamic field ($\varphi = 90°$), vary the frequency $f$ of the dynamic field in a broad range, and record the rf-induced BLS intensity for each excitation frequency. The resonant spectrum obtained for the 500-nm disk at $H_0 = 20$ mT and $P = 0.2$ mW is plotted on a logarithmic scale in Fig. 1(b). Despite the poor coupling of the uniform excitation field with nonuniform spin-wave modes, up to eight peaks can be detected in the spectrum. To identify the observed modes, we calculate the frequencies and spatial profiles of the eigenmodes of the disk using an eigenmode solver [38]. In these calculations, we use the independently determined saturation magnetization of 176 mT and standard-for-YIG exchange constant of 3.6 pJ/m. Because of the small diameter of the disk, the modes are well separated in the frequency space. Therefore, it is easy to associate the frequencies obtained from the calculations [vertical lines in Fig. 1(b)] with the frequencies of the peaks observed in the experiment. All the computed mode frequencies match well with the measured frequencies, except for the first-two lowest-frequency modes. As seen from the computed mode profiles in Fig. 1(b), these are the modes strongly localized at the edges of the disk — edge modes. We note that this is a generic feature of edge modes to be very sensitive to the conditions at the edges [39]. As a result, their quantitative characteristics typically cannot be reproduced in calculations with ideal edges [40–42]. Nevertheless, from comparison of the experimental spectrum with the calculated spectrum, it is reasonable to associate the two peaks at frequencies of 1.30 and 1.36 GHz with the edge modes of the disk. In contrast, the identification of the bulk modes is straightforward. These modes can be labeled with the number of lobes $(n_{\parallel}, n_{\perp})$ of the standing waves in the directions parallel and transverse to the in-plane static magnetic field $H_0$. The first-three calculated modes of the $n_{\perp} = 1$ branch have frequencies $f_{1,1} = 1.63$ GHz, $f_{2,1} = 1.67$ GHz, and $f_{3,1} = 1.91$ GHz, which agree well with the frequencies of the observed

peaks of 1.64, 1.70, and 1.94 GHz. The calculated frequency of the mode (1,2) $f_{1,2} = 2.19$ GHz belonging to the branch $n_{\perp} = 2$ coincides with the detected frequency of the peak at 2.19 GHz, and the frequencies of the modes (1,3) $f_{1,3} = 2.59$ GHz and (2,3) $f_{2,3} = 2.55$ GHz belonging to the branch $n_{\perp} = 3$ fit the frequencies of the BLS peaks at 2.61 and 2.55 GHz.

## III. RESULTS AND DISCUSSION

We now investigate the parametric excitation of the modes using high-amplitude dynamic fields. First, we address the well-studied case of the parallel pumping corresponding to the geometry where the static magnetic field is oriented parallel to the dynamic excitation field $h_{\mathrm{rf}}$ ($\varphi = 0$). Under these conditions, no direct linear coupling of the excitation field with the dynamic magnetization is possible. Instead, the magnetization dynamics can be driven by the parametric mechanism. Because of the presence of the dynamic magnetic field, $h_{\mathrm{rf}}$, parallel to the static magnetic field $H_0$, the latter becomes periodically modulated in time. As in the general case of a harmonic oscillator with a periodically modulated parameter, dynamical states can be excited when the amplitude of the modulation is sufficiently large and the frequency of the modulation is twice the resonant frequency of the system. In the case of magnetic systems, this process can also be considered as the splitting of a photon at the pumping frequency into two magnons with frequencies twice as small [12].

Figure 2(a) shows a representative BLS spectrum of magnetic oscillations recorded by applying the rf current with power $P = 2$ mW at pumping frequency $f_{\mathrm{p}} = 3.28$ GHz, which is twice the frequency of the fundamental (1,1) mode of the disk, 1.64 GHz [see Fig. 1(b)]. As seen from Fig. 2(a), in agreement with the expectations, pumping efficiently excites the mode at $f_{\mathrm{p}}/2$. Figure 2(b) combines in a color map the BLS spectra measured for pumping frequencies ranging from 2.4 to 4.8 GHz. These data clearly show that parallel pumping results in the excitation of degenerate magnon pairs at exactly $f_{\mathrm{p}}/2$ (dashed white line), when this frequency coincides with the frequency of one of the resonant modes of the disk. Since the parametric process is not limited by the spatial profile of the excitation field, many more modes can be excited in comparison with the case of linear excitation [Fig. 1(b)]. Additionally, since the parametric process is a threshold phenomenon, the number of excited modes depends on the pumping power. This is demonstrated in Fig. 2(c), which shows the power dependence of the intensity of the modes labeled as "A," "B," and "C" in Fig. 2(b). In particular, mode C can be excited only at $P > 1$ mW, while mode A exhibits nonzero intensity already at $P = 0.05$ mW. The threshold power is proportional to the ratio of the relaxation frequency to the ellipticity [12,27]. As the relaxation
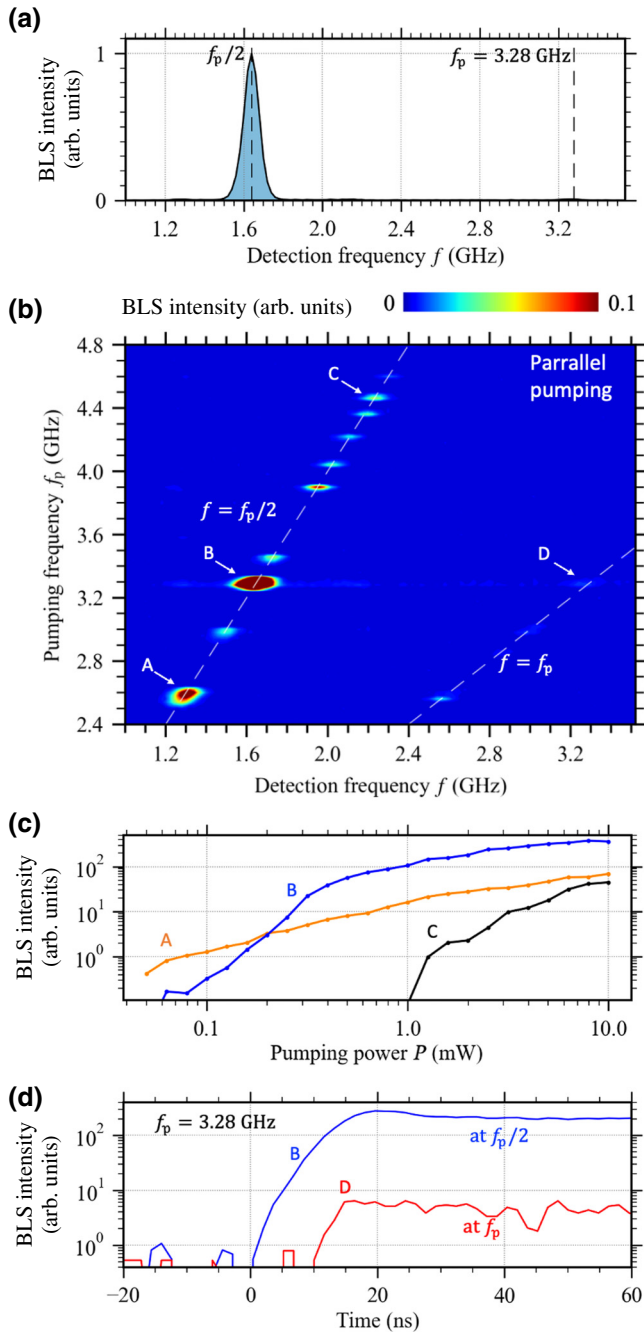
FIG. 2.   (a) Representative BLS spectrum of parametrically excited magnetic oscillations recorded at pumping frequency $f_p = 3.28$ GHz and pumping power $P = 2$ mW. (b) BLS spectra measured for pumping frequency $f_p$ ranging from 2.4 to 4.8 GHz combined in a linear-scale color map. Color interpolation is used to improve readability. (c) Power dependences of the intensity of the modes labeled "A," "B," and "C" in (b). (d) Temporal dependences of the modes labeled "B" and "D" in (b) measured at $P = 10$ mW. The data were obtained at $H_0 = 20$ mT and $\varphi = 0°$ (parallel-pumping geometry) on the $D = 0.5$ μm disk.

frequency increases and the ellipticity of the modes tends to decrease with increased $n_{||}$ and $n_\perp$, the threshold tends to increase with frequency.

We emphasize that although the number of excited modes increases with the pumping power, the process remains degenerate at all powers. In other words, by the use of pumping with a fixed frequency, only one mode can be excited at a time. A careful examination of the data in Fig. 2(b) shows that, in addition to the signal at $f_p/2$, one also observes a weak signal at $f_p$ (e.g., mode labeled "D"). This weak, additional excitation appears only if the amplitude of the mode at $f_p/2$ is large and, therefore, is not associated with the direct excitation of magnetization dynamics by the pumping. Moreover, time-resolved BLS measurements show that the signal at $f_p/2$ precedes the signal at $f_p$ in time [Fig. 2(d)], which is a clear indication that the signal at $f_p$ is caused by the parametrically excited dynamics at $f_p/2$, and not vice versa. We associate this signal with a nonresonant second-harmonic generation [43].

Let us now return to the configuration of transverse pumping ($\varphi = 90°$), which we used earlier for linear excitation [Fig. 1(b)], and apply an excitation field at frequencies twice the frequencies of the detected modes. Under these conditions, the excitation field can linearly excite magnetization dynamics. However, the resonant modes available at these frequencies possess very large effective wave vectors and do not couple efficiently to the uniform dynamic field. Therefore, the nonresonant excitation dominates in this regime. The dynamic magnetic field $h_{rf}$ directly excites a quasiuniform magnetization precession at the frequency $f_p$, which can be considered as the excitation of a nonresonant magnon. Similarly to resonant magnons, at sufficiently large powers, the nonresonant magnon at $f_p$ can split into two magnons with frequencies $f_1$ and $f_2$: $f_1 + f_2 = f_p$. Moreover, as in the case of resonant magnons [30–32], this process is expected to be nondegenerate, i.e., $f_1 \neq f_2$.

Figure 3(a) shows a representative BLS spectrum recorded at $f_p = 3.48$ GHz and $P = 5$ mW. In contrast to the spectrum for the case of parallel pumping [Fig. 2(a)], the spectrum in Fig. 3(a) exhibits a well-pronounced peak at $f_p$ (labeled "B") reflecting the nonresonant excitation of magnetization dynamics at this frequency. As clearly seen from Fig. 3(a), nonresonantly excited magnons B do not split into magnons at $f_p/2$. Instead, a nondegenerate magnon pair (A1, A2) at $f_p/2 \pm \delta f$ is excited, where $\delta f = 0.44$ GHz. The frequencies of the excited modes A1 (1.3 GHz) and A2 (2.18 GHz) correspond to the previously identified first edge mode and the (1,2) mode. Figure 3(b) combines in a color map the BLS spectra measured for pumping frequency ranging from 2.8 to 4.8 GHz. As can be seen from these data, in the geometry of transverse pumping, parametric excitation has a nondegenerate character for all the observed splitting processes: there is no signature of dynamics excited at frequency $f = f_p/2$. Additionally, in accordance with expectations, we observe excitation at $f = f_p$ over the entire range studied, which is in strong contrast to the case of parallel pumping [Fig. 2(b)].

To get better insight into the nondegenerate splitting processes, we mark in Fig. 3(b) the experimentally resolved frequencies of the modes [Fig. 1(b)]. From this analysis one can observe that many observed mode pairs include at least one edge mode. This is associated with their strong spatial localization resulting in a wide distribution in the reciprocal space, which helps to fulfill the linear-momentum conservation law in magnon splitting processes [44]. We emphasize, however, that the eigenmodes of an in-plane saturated magnetic disk are far from being a simple combination of standing plane waves [see the mode profiles in Fig. 1(b)]. Therefore, even bulk modes are characterized by a wide distribution in the momentum space, which facilitates the fulfilment of the momentum conservation [33,44]. As shown below, in larger disks, where the mode spectrum is much denser in the frequency space, pairs of bulk modes can also be easily excited.

To compare the efficiency of the nondegenerate transverse-pumping process with efficiency in the parallel-pumping case, we find the threshold power necessary to excite the most-intense pair, labeled in Fig. 3(b) as "A1" and "A2." The power dependence of the intensities of these modes is plotted in Fig. 3(c). We emphasize that the apparent difference in the intensities of the modes forming a pair [see Fig. 3(a)] originates from the different sensitivity of the optical setup to different modes. Therefore, we renormalize the dependence for mode A2 to match the intensity of mode A1 [in Fig. 3(c) we choose a normalization factor that is 15% off its nominal value to improve readability]. The perfect match between the two curves indicates that both modes are excited simultaneously and possess the same excitation threshold, as expected for a nondegenerate three-magnon process. This threshold, 0.4 mW, is larger than that for mode A in Fig. 2(c), which corresponds to mode A1 of the pair. However, it is more than twice as small as the threshold for mode C in Fig. 2(c), which corresponds to mode A2. In other words, despite the need for nonresonant excitation, the efficiency of the transverse-pumping parametric process is comparable to that of the parallel-pumping process. A possible approach to further increase the efficiency is based on the use of magnetic systems that combine two materials with different saturation magnetization, where transverse pumping resonantly excites magnons in one material, which then parametrically excite magnon pairs in the other material [45].

Let us now turn to the temporal characteristics of the nondegenerate process. Figure 3(d) shows the temporal dependence of the intensities of modes A1 and A2 together with the dependence of the intensity of oscillations at the pumping frequency $f_p$ [labeled "B" in Fig. 3(b)]. First, one can see that rise time of the intensities of modes A1 and A2 until the steady state is reached is noticeably longer than in the case of the parallel-pumping excitation [Fig. 2(d)]. Second, in strong contrast to the parallel-pumping case, the signal at $f_p/2 \pm \delta f$ is delayed with respect to the
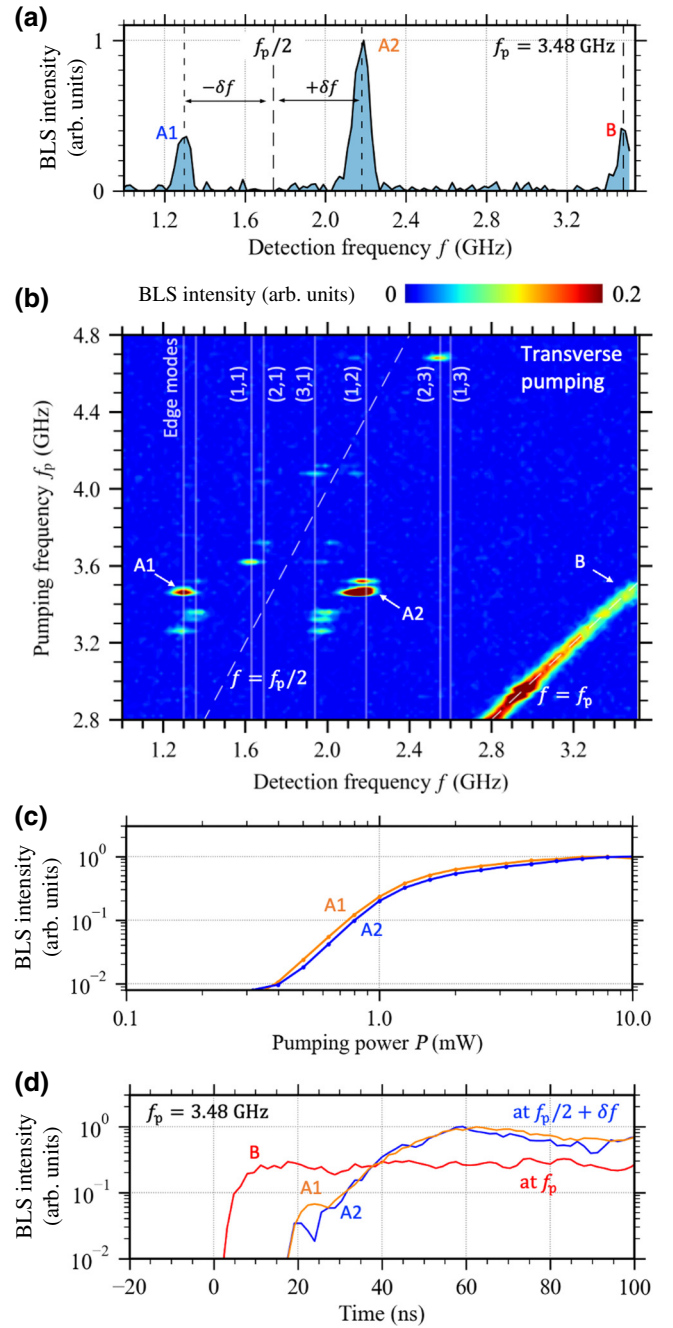


FIG. 3. (a) Representative BLS spectrum of parametrically excited magnetic oscillations recorded at pumping frequency $f_p = 3.48$ GHz and pumping power $P = 5$ mW. (b) BLS spectra measured for pumping frequency $f_p$ ranging from 2.8 to 4.8 GHz combined in a linear-scale color map. Color interpolation is used to improve readability. Vertical lines mark the experimentally detected frequencies of the eigenmodes. Labeling of the modes is based on a comparison of measured and calculated frequencies, as discussed in the text. (c) Power dependences of the intensity of the modes labeled "A1" and "A2" in (b). (d) Temporal dependences of the modes labeled "A1," "A2," and "B" in (b) measured at $P = 10$ mW. The data were obtained at $H_0 = 20$ mT and $\varphi = 90°$ (transverse-pumping geometry) on the $D = 0.5\,\mu\text{m}$ disk.
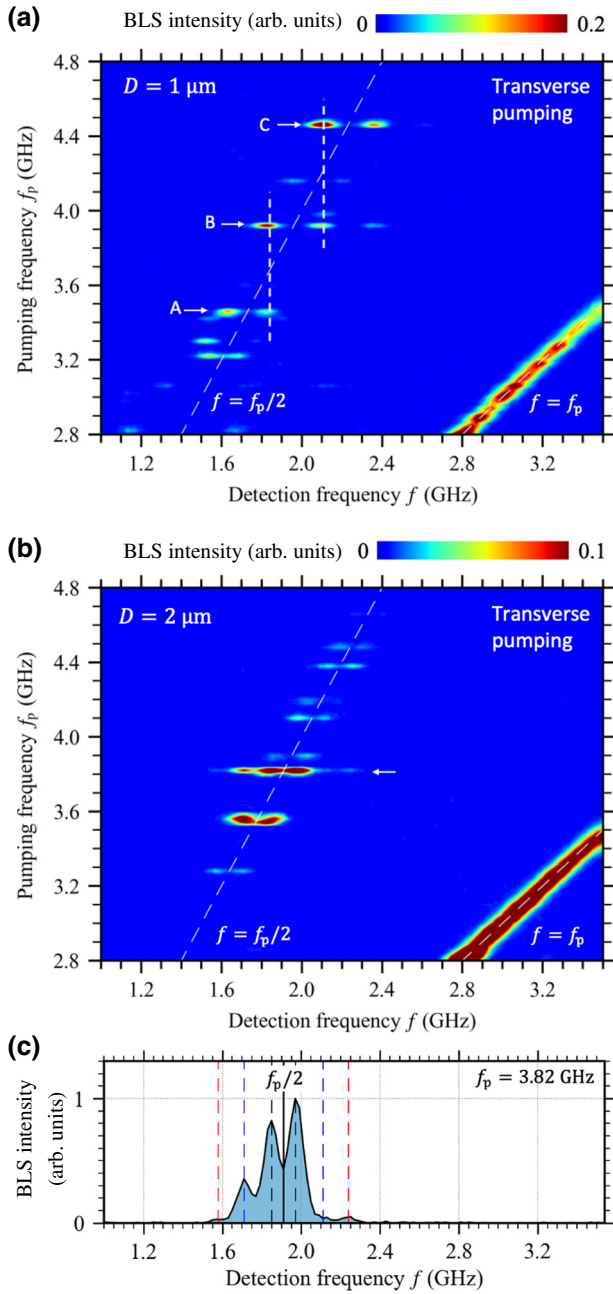
FIG. 4. (a),(b) BLS spectra measured for pumping frequency $f_p$ ranging from 2.8 to 4.8 GHz combined in a linear-scale color map. Color interpolation is used to improve readability. (a) $D = 1\,\mu m$ and (b) $D = 2\,\mu m$. "A", "B" and "C" indicate the 3 pairs of modes excited for a pumping frequency $f_p$ of 3.46, 3.92 and 4.46 GHz respectively. Vertical dashed lines in (a) mark the frequencies of the modes common for pairs A, B, and C. (c) BLS spectrum recorded for the 2-$\mu m$ disk at $f_p = 3.48$ GHz, as marked by an arrow in (b). The data were obtained at $P = 5$ mW, $H_0 = 20$ mT, and $\varphi = 90°$ (transverse-pumping geometry).

signal at $f_p$. This reflects the two-stage nature of the transverse-pumping process, which requires the excitation of an intense nonresonant dynamic magnetic state as an intermediate step. We note, however, that the settling times are of the same order of magnitude. Additionally, they can be reduced by further increase of the pumping power.

We now discuss the effect of the disk size on the excitation of nondegenerate pairs. Figures 4(a) and 4(b) show the excitation maps for the disks with diameter $D$ of 1 and 2 $\mu m$, respectively. As seen from these data, more pairs can be excited in larger disks, and most observed pairs belong to the frequency range of bulk modes. This is associated with the decrease in the mode separation in the frequency space with increasing diameter $D$, which also results in a decrease of the characteristic frequency separation in individual pairs, $2\delta f$. In particular, for $D = 1\,\mu m$, $2\delta f \approx 0.2$ GHz, and for $D = 2\,\mu m$, $2\delta f \approx 0.1$ GHz, i.e., the frequency separation is inversely proportional do the disk size. Because of the denser mode spectrum, in larger disks, one can easily find pairs that share the same mode, e.g., pairs A + B and B + C in Fig. 4(a). If such pairs are driven simultaneously by a multifrequency pumping field, one can expect cross-stimulation of splitting processes, as was previously observed for resonant three-magnon splitting in the vortex state [11]. This opens, for example, the possibility to significantly expand the range of materials and geometries for implementation of the nontraditional computing scheme proposed in Ref. [11]. Additionally, many of the modes belonging to the observed pairs can be easily excited with the use of a linear-excitation mechanism, which provides additional means to control the system of interacting modes. Moreover, because of the dense spectrum of modes in sufficiently large disks, it is possible to simultaneously fulfill the energy-conservation conditions for several pairs. As a result, one can excite multiple pairs using a single-frequency transverse pumping. This is demonstrated in Fig. 4(c), which shows the BLS spectrum recorded for a 2-$\mu m$ large disk driven by pumping at $f_p = 3.82$ GHz [also marked with an arrow in Fig. 4(b)]. As seen from these data, up to three mode pairs (six different modes) can be simultaneously excited in this system. Note that the peak at 2.1 GHz is not well resolved, likely due to the low sensitivity of BLS spectroscopy to the corresponding mode. However, knowing that the peaks always appear in pairs centered at $f_p/2$, one can assume with a high degree of confidence that the increased intensity at 2.1 GHz indicates the presence of excitation at this frequency.

## IV. CONCLUSIONS

In conclusion, we have shown that a microscopic system based on a promising low-damping magnetic insulator, in the uniform ferromagnetic state, can demonstrate degenerate and nondegenerate parametric phenomena that can be controlled by varying the relative orientation of the pumping field and the static magnetization. In particular, nonresonant transverse parametric pumping allows one to

efficiently excite nondegenerate pairs of magnons without the requirement of engineering the presence of low-order resonant modes at twice the center frequency of the pair. Getting rid of this limiting prerequisite represents a new paradigm for nondegenerate parametric processes that have been underutilized in thin ferromagnetic films such as YIG. These nondegenerate processes demonstrate two key properties: (1) one mode can be addressed by multiple independent pumping frequencies and (2) pairs of modes can be excited with a single frequency that effectively couples the modes of the pair. These properties are of decisive importance to implement novel hardware platforms for nonconventional computing and data processing relying on modes interacting in the reciprocal space. In this paradigm, magnetic modes would assume the role of neurons, and energy (and momentum) transfer from mode to mode can be accomplished through synaptic weights that can be mapped to nonlinear processes such as those exemplified in the present work. Our findings show that practical implementation of such systems is not limited to specific static magnetic configurations and materials but can greatly benefit from the versatile nonlinear processes present in low-damping thin magnetic materials, which is expected to facilitate further development in the field of magnonic neuromorphic computing.

## ACKNOWLEDGMENTS

[1] A. Khitun, M. Bao, and K. L. Wang, Magnonic logic circuits, J. Phys. D: Appl. Phys. **43**, 264005 (2010).

[2] G. Csaba, Á Papp, and W. Porod, Perspectives of using spin waves for computing and signal processing, Phys. Lett. A **381**, 1471 (2017).

[3] A. Mahmoud, F. Ciubotaru, F. Vanderveken, A. V. Chumak, S. Hamdioui, C. Adelmann, and S. Cotofana, Introduction to spin wave computing, J. Appl. Phys. **128**, 161101 (2020).

[4] A. V. Chumak, P. Kabos, M. Wu, C. Abert, C. Adelmann, A. O. Adeyeye, J. Åkerman, F. G. Aliev, A. Anane, A. Awad, C. H. Back, *et al.*, Advances in magnetics roadmap on spin-wave computing, IEEE Trans. Magn. **58**, 1 (2022).

[5] R. Nakane, G. Tanaka, and A. Hirose, Reservoir computing with spin waves excited in a garnet film, IEEE Access **6**, 4462 (2018).

[6] T. W. Hughes, I. A. D. Williamson, M. Minkov, and S. Fan, Wave physics as an analog recurrent neural network, Sci. Adv. **5**, eaay6946 (2019).

[7] M. Zahedinejad, A. A. Awad, S. Muralidhar, R. Khymyn, H. Fulara, H. Mazraati, M. Dvornik, and J. Åkerman, Two-dimensional mutually synchronized spin Hall nano-oscillator arrays for neuromorphic computing, Nat. Nanotechnol. **15**, 47 (2020).

[8] A. Papp, W. Porod, and G. Csaba, Nanoscale neural network using non-linear spin-wave interference, Nat. Commun. **12**, 6422 (2021).

[9] A. A. Nikitin, A. A. Nikitin, A. B. Ustinov, S. Watt, and M. P. Kostylev, Theoretical model for nonlinear spin-wave transient processes in active-ring oscillators with variable gain and its application for magnonic reservoir computing, J. Appl. Phys. **131**, 113903 (2022).

[10] J. C. Gartside, K. D. Stenning, A. Vanstone, H. H. Holder, D. M. Arroo, T. Dion, F. Caravelli, H. Kurebayashi, and W. R. Branford, Reconfigurable training and reservoir computing in an artificial spin-vortex ice via spin-wave fingerprinting, Nat. Nanotechnol. **17**, 460 (2022).

[11] L. Körber, C. Heins, T. Hula, J.-V. Kim, S. Thlang, H. Schultheiss, J. Fassbender, and K. Schultheiss, Pattern recognition in reciprocal space with a magnon-scattering reservoir, Nat. Commun. **14**, 3954 (2023).

[12] G. A. Melkov and A. G. Gurevich, *Chapter 10 — Parametric Excitation of Magnetic Oscillations and Waves, in Magnetization Oscillations and Waves* (CRC Press, New York, 1996), pp. 245–282.

[13] V. E. Zakharov, V. S. L'vov, and S. S. Starobinets, Spin-wave turbulence beyond the parametric excitation threshold, Sov. Phys. Usp. **17**, 896 (1975).

[14] H. Kurebayashi, O. Dzyapko, V. E. Demidov, D. Fang, A. J. Ferguson, and S. O. Demokritov, Spin pumping by parametrically excited short-wavelength spin waves, Appl. Phys. Lett. **99**, 162502 (2011).

[15] C. W. Sandweg, Y. Kajiwara, A. V. Chumak, A. A. Serga, V. I. Vasyuchka, M. B. Jungfleisch, E. Saitoh, and B. Hillebrands, Spin pumping by parametrically excited exchange magnons, Phys. Rev. Lett. **106**, 216601 (2011).

[16] A. A. Serga, C. W. Sandweg, V. I. Vasyuchka, M. B. Jungfleisch, B. Hillebrands, A. Kreisel, P. Kopietz, and M. P. Kostylev, Brillouin light scattering spectroscopy of parametrically excited dipole-exchange magnons, Phys. Rev. B **86**, 134403 (2012).

[17] C. Hahn, G. de Loubens, M. Viret, O. Klein, V. V. Naletov, and J. Ben Youssef, Detection of microwave spin pumping using the inverse spin Hall effect, Phys. Rev. Lett. **111**, 217204 (2013).

[18] V. Lauer, D. A. Bozhko, T. Brächer, P. Pirro, A. A. Serga, M. B. Jungfleisch, M. Agrawal, G. A. Melkov, B. Hillebrands, A. V. Chumak, *et al.*, Spin-transfer torque based damping control of parametrically excited spin waves in a magnetic insulator, Appl. Phys. Lett. **108**, 012402 (2016).

[19] T. Brächer, P. Pirro, and B. Hillebrands, Parallel pumping for magnon spintronics: Amplification and manipulation of magnon spin currents on the micron-scale, Phys. Rep. **699**, 1 (2017).

[20] M. Mohseni, M. Kewenig, R. Verba, Q. Wang, M. Schneider, B. Heinz, A. A. Serga, B. Hillebrands, A. V. Chumak, P. Pirro, *et al.*, Parametric generation of propagating spin waves in ultrathin yttrium iron garnet waveguides, Phys. Status Solidi RRL **14**, 2000011 (2020).

[21] S. Hwang, S. Yoon, D. Seo, S. H. Han, and B. K. Cho, Parametric excitation and mode control using an Oersted field in a NiFe nanowire, Sci. Rep. **11**, 1 (2021).

[22] B. Heinz, M. Mohseni, A. Lentfert, R. Verba, M. Schneider, B. Lägel, K. Levchenko, T. Brächer, C. Dubs, A. V. Chumak, and P. Pirro, Parametric generation of spin waves in nanoscaled magnonic conduits, Phys. Rev. B **105,** 144424 (2022).

[23] S. Urazhdin, V. Tiberkevich, and A. Slavin, Parametric excitation of a magnetic nanocontact by a microwave field, Phys. Rev. Lett. **105,** 237204 (2010).

[24] Y.-J. Chen, H. K. Lee, R. Verba, J. A. Katine, I. Barsukov, V. Tiberkevich, J. Q. Xiao, A. N. Slavin, and I. N. Krivorotov, Parametric resonance of magnetization excited by electric field, Nano Lett. **17,** 572 (2017).

[25] H. Ulrichs, V. E. Demidov, S. O. Demokritov, and S. Urazhdin, Parametric excitation of eigenmodes in microscopic magnetic dots, Phys. Rev. B **84,** 094401 (2011).

[26] E. R. J. Edwards, H. Ulrichs, V. E. Demidov, S. O. Demokritov, and S. Urazhdin, Parametric excitation of magnetization oscillations controlled by pure spin current, Phys. Rev. B **86,** 134420 (2012).

[27] F. Guo, L. M. Belova, and R. D. McMichael, Parametric pumping of precession modes in ferromagnetic nanodisks, Phys. Rev. B **89,** 104422 (2014).

[28] T. Srivastava, H. Merbouche, I. Ngouagnia Yemeli, N. Beaulieu, J. Ben Youssef, M. Muñoz, P. Che, P. Bortolotti, V. Cros, O. Klein, G. de Loubens, *et al.*, Identification of a large number of spin-wave eigenmodes excited by parametric pumping in yttrium iron garnet microdisks, Phys. Rev. Appl. **19,** 064078 (2023).

[29] V. V. Naletov, G. de Loubens, G. Albuquerque, S. Borlenghi, V. Cros, G. Faini, J. Grollier, H. Hurdequint, N. Locatelli, B. Pigeau, *et al.*, Identification and selection rules of the spin-wave eigenmodes in a normally magnetized nanopillar, Phys. Rev. B **84,** 224423 (2011).

[30] A. Melkov and S. V. Sholom, Parametric excitation of spin waves by a surface magnetostatic wave, Zh. Eksp. Teor. Fiz. **96,** 712 (1989).

[31] K. Schultheiss, R. Verba, F. Wehrmann, K. Wagner, L. Körber, T. Hula, T. Hache, A. Kákay, A. A. Awad, V. Tiberkevich, *et al.*, Excitation of whispering gallery magnons in a magnetic vortex, Phys. Rev. Lett. **122,** 097202 (2019).

[32] L. Körber, C. Heins, I. Soldatov, R. Schäfer, A. Kákay, H. Schultheiss, and K. Schultheiss, Modification of three-magnon splitting in a flexed magnetic vortex, Appl. Phys. Lett. **122,** 092401 (2023).

[33] R. Verba, L. Körber, K. Schultheiss, H. Schultheiss, V. Tiberkevich, and A. Slavin, Theory of three-magnon interaction in a vortex-state magnetic nanodot, Phys. Rev. B **103,** 014413 (2021).

[34] H. Yu, O. d'Allivy Kelly, V. Cros, R. Bernard, P. Bortolotti, A. Anane, F. Brandl, R. Huber, I. Stasinopoulos, and D. Grundler, Magnetic thin-film insulator with ultra-low spin wave damping for coherent nanomagnonics, Sci. Rep. **4,** 6848 (2014).

[35] C. Hauser, T. Richter, N. Homonnay, C. Eisenschmidt, M. Qaid, H. Deniz, D. Hesse, M. Sawicki, S. G. Ebbinghaus, and G. Schmidt, Yttrium iron garnet thin films with very low damping obtained by recrystallization of amorphous material, Sci. Rep. **6,** 20827 (2016).

[36] N. Beaulieu, N. Kervarec, N. Thiery, O. Klein, V. Naletov, H. Hurdequint, G. de Loubens, J. B. Youssef, and N. Vukadinovic, Temperature dependence of magnetic properties of a ultrathin yttrium-iron garnet film grown by liquid phase epitaxy: Effect of a Pt overlayer, IEEE Magn. Lett. **9,** 1 (2018).

[37] V. E. Demidov and S. O. Demokritov, Magnonic waveguides studied by microfocus Brillouin light scattering, IEEE Trans. Magn. **51,** 1 (2015).

[38] M. d'Aquino, C. Serpico, G. Miano, and C. Forestiere, A novel formulation for the numerical computation of magnetization modes in complex micromagnetic systems, J. Comput. Phys. **228,** 6130 (2009).

[39] R. D. McMichael and B. B. Maranville, Edge saturation fields and dynamic edge modes in ideal and nonideal magnetic film edges, Phys. Rev. B **74,** 024424 (2006).

[40] F. Guo, L. M. Belova, and R. D. McMichael, Spectroscopy and Imaging of Edge Modes in Permalloy Nanodisks, Phys. Rev. Lett. **110,** 017601 (2013).

[41] Z. Duan, A. Smith, L. Yang, B. Youngblood, J. Lindner, V. E. Demidov, S. O. Demokritov, and I. N. Krivorotov, Nanowire spin torque oscillator driven by spin orbit torques, Nat. Commun. **5,** 1 (2014).

[42] Z. Duan, I. N. Krivorotov, R. E. Arias, N. Reckers, S. Stienen, and J. Lindner, Spin wave eigenmodes in transversely magnetized thin film ferromagnetic wires, Phys. Rev. B **92,** 104424 (2015).

[43] V. E. Demidov, M. P. Kostylev, K. Rott, P. Krzysteczko, G. Reiss, and S. O. Demokritov, Generation of the second harmonic by spin waves propagating in microscopic stripes, Phys. Rev. B **83,** 054408 (2011).

[44] A. Etesamirad, J. Kharlan, R. Rodriguez, I. Barsukov, and R. Verba, Controlling selection rules for magnon scattering in nanomagnets by spatial symmetry breaking, Phys. Rev. Appl. **19,** 044087 (2023).

[45] L. Sheng, M. Elyasi, J. Chen, W. He, Y. Wang, H. Wang, H. Feng, Y. Zhang, G. E. Bauer, H. Yu, *et al.*, Nonlocal detection of interlayer three-magnon coupling, Phys. Rev. Lett. **130,** 046701 (2023).